Deep crustal fracture zones control fluid escape and the seismic cycle in the Cascadia subduction zone

Benoît Tauzin *, Bruno Reynard, Jean-Philippe Perrillat, Eric Debayle, Thomas Bodin

Laboratoire de Géologie de Lyon, Terre, Planètes, Environnement, Université de Lyon, Ecole Normale Supérieure de Lyon, CNRS UMR 5276, 2 rue Raphael Dubois, 69622 Villeurbanne Cedex, France

ABSTRACT

Seismic activity and non-volcanic tremors are often associated with fluid circulation resulting from the dehydration of subducting plates. Tremors in the overriding continental crust of several subduction zones suggest fluid circulation at shallower depths, but potential fluid pathways are still poorly documented. Using receiver function analysis in the Cascadia subduction zone, we provide evidence for a seismic discontinuity near 15 km depth in the crust of the overriding North American plate. This interface is segmented, and its interruptions are spatially correlated with conductive regions of the forearc and shallow swarms of seismicity and non-volcanic tremors. These observations suggest that fluid circulation in the overriding plate is controlled by fault zones separating blocks of accreted terranes. These zones constitute fluid escape routes that may influence the seismic cycle by releasing fluid pressure from the megathrust.

© 2016 Elsevier B.V. All rights reserved.

1. Introduction

Along the Cascadia subduction margin, the oceanic Gorda–Juan de Fuca (JdF) plate has underthrusted the continental North American (NA) plate over the last 6–10 Myr (Fig. 1). A first order and largely debated question concerns the recurrence as well as the spatial distribution of large earthquakes on the megathrust of this subduction zone (*e.g.* Hyndman, 2013). Paleo-seismological reconstructions of recorded subsidence in coastal intertidal marshes suggest a northward increase of recurrence intervals from ∼230 yr to ∼480 yr (Leonard et al., 2010). Modeling of coseismic subsidence of the 1700 A.D. great Cascadia earthquake (Wang et al., 2013) implies a seismic rupture in a single magnitude 9.0 event of much if not the whole length of the margin. The modeling revealed along-strike slip heterogeneities, with patches of higher-moment release separated by an area of lower-moment release near Alsea Bay in Oregon (∼44.4°N). This heterogeneous short-term frictional behavior on the megathrust is also predicted by a recent local gps geodetical study (Schmalzle et al., 2014). The modeled locked zones reveal a wider transition zone under central Oregon than in nearby regions of northern California, Washington, and the Vancouver island, further suggesting that the frictional behav-

ior is segmented along the Cascadia margin. Aseismic slip events, non-volcanic tremors, and low-frequency earthquakes, are also the manifestation of the short-term frictional behavior on the subduction megathrust (Dragert et al., 2001; Rogers and Dragert, 2003; Shelly et al., 2006). Along-strike variations in the distribution and recurrence interval of episodic tremors and aseismic slips, in correlation with the location of forearc basins interpreted as the manifestation of megathrust asperities, have lead Brudzinski and Allen (2007) to speculate a possible link between the long- and short-term seismic cycles. The exact nature of this link still remains to be clearly demonstrated.

The strength of faults, and in particular that of the subduction megathrust where major earthquakes occur, is influenced by the build-up and release of pore-fluid pressure near the slab interface. Fluids originate from metamorphic dehydration reactions in the subducting plate (Hacker et al., 2003). In a partially sealed fault zone, water is extracted from minerals faster than it can be removed by porous flow. This increases the fluid pressure on the megathrust so that frictional earthquake failure occurs at low shear stress (Sleep and Blanpied, 1992). In this way, at the plate interface, fluid pressure is believed to control the occurrence of earthquakes, episodic tremors, and aseismic slip (Obara, 2002; Hacker et al., 2003; Rogers and Dragert, 2003; Audet et al., 2009). Diffuse seismic activity in the overriding plate has also been associated with fluid circulation (Kao et al., 2005; Reyners and Eberhart-Phillips, 2009) but neither the fluid paths
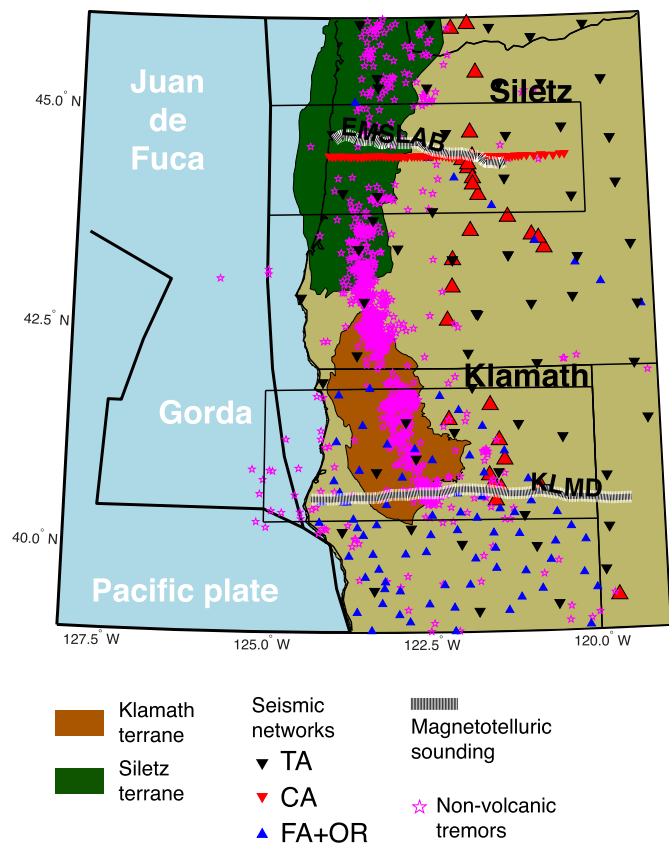
Fig. 1. The geodynamical and geological context of the studied area with the locations of the Siletz and Klamath geological terranes in Oregon and California (Ernst et al., 2008; McCrory and Wilson, 2013). Small triangles are three-component broadband seismological stations. The seismic networks used in this study are the Transportable Array (TA), the Mendocino and Oregon Teleseismic Experiments (FA+OR), and the Cascadia 93 experiment (CA). The areas sampled by the seismic data in Figs. 5 and 6 are indicated with the black frames. The hatched thick white lines correspond to the magnetotelluric survey lines of Wannamaker et al. (2014). The non-volcanic tremors (magenta stars) are from a catalog of Idehara et al. (2014). (For interpretation of the references to color in this figure legend, the reader is referred to the web version of this article.)

nor the structural control of the overlying forearc geological terranes have truly been evidenced.

In Cascadia, the JdF plate subducts below island arc-subduction assemblages of volcanic rocks that provide the basement throughout much of the arc and forearc (Fig. 1). In central Oregon, the Siletz terrane basalts that are Paleocene to Eocene in age underlie the Coastal Range as well as the western part of the Willamette Basin. In northern California and southern Oregon, much of the forearc is covered by Mesozoic and Paleozoic metamorphic, volcanic, and plutonic basement blocks, the Klamath terranes. By their composition and morphology, these terranes are the usual suspects for controlling the strength variations and the seismic cycle on the megathrust (Brudzinski and Allen, 2007; Audet and Bürgmann, 2014; Wannamaker et al., 2014; Schmalzle et al., 2014). In this study, combining the information provided by high-resolution seismic imaging with electrical resistivity profiles from Wannamaker et al. (2014) sensitive to the amount and nature of fluids, we provide evidence for deep crustal fracture zones in the terranes of the Cascadia forearc. The extent of the fracture zones could control the permeability properties of the forearc, and may determine the presence of shallow non-volcanic tremors. Fluctuations in pore-fluid pressure due to heterogeneous distribution of fractures could also contribute to the segmentation of frictional behavior along the Cascadia margin.

2. Data and methods

We conducted a new analysis of receiver functions (RFs) from two previous studies including data from the Earthscope Transportable Array (Tauzin et al., 2013), and two denser arrays in central Oregon and northern California, the Cascadia 93 and the FAME Mendocino experiments (Tauzin et al., 2016). This comprehensive database of 82,885 RFs allows the dense coverage of a region of approximatively 300×600 km^2 in the arc and forearc of the Cascadia subduction zone (Fig. 1).

The RFs are the records of P-to-S converted waves that reverberate in the structure beneath seismometers and are isolated from the primary incident teleseismic P-wave by deconvolution (Ammon, 1991). We computed the RFs after rotation of the recording components into the Z-R-T directions, using different low-pass filters at 1 and 0.2 Hz, and using an iterative time–domain deconvolution (Ligorrìa and Ammon, 1999).

We used a common conversion point stacking approach (CCP), which back-projects the seismic signal recorded on the RFs at the corresponding location of theoretical scatterers in the subsurface (e.g. Zhu, 2000; Wittlinger et al., 2004). We used the one-dimensional IASP91 velocity model (Kennett and Engdahl, 1991) for ray-tracing and time-to-depth conversion. In Oregon, where the dense Cascadia 93 network is available with inter-station distances of ~5 km, we stacked the data sensitive to the structure within a distance of 20 km around the profile, and projected them onto the 2D vertical profile. In California where the Mendocino network is sparser (25 km average station spacing), we stacked and projected the data from stations within 100 km of the profile to benefit from data redundancy and improve the signal-to-noise ratio. These lateral distances of projection are reduced compared with our previous work at larger scale (Tauzin et al., 2013; Tauzin et al., 2016, used a ±250 km lateral distance of projection).

Our images are then built from multi-mode CCP stacking (Hetényi, 2007; Tauzin et al., 2016) by combining three images using the PS, PPS, and PSS modes of scattering (Fig. 2). By taking explicitly into account seismic phases reflected multiple times (i.e. second order scattering effects), this method removes artifacts from multiples and significantly improves the resolution and the signal-to-noise ratio (Bostock et al., 2002; Tauzin et al., 2016). The PS modes are conversions from P-waves to S-waves (Fig. 2a). PPS and PSS are multiple reverberated waves (Fig. 2b, c). The time-to-depth conversion of the multiples warps more the RF signal than does the back-projection for the PS signal. Therefore to turn the images to similar wavelengths, the data are filtered with low-pass corner frequencies at 1 Hz for PS, and 0.2 Hz for PPS and PSS (Tauzin et al., 2016). We also reversed in polarity the PSS image because PSS conversions have opposite amplitudes to the PS and PPS modes (Fig. 2c). The final multi-mode images in Fig. 2d are simply constructed by stacking the three images obtained from the different modes. To remove possible problems arising from stacking out phase modes, we proceed to a phase-weighted stack (Schimmel and Paulssen, 1997). The operation efficiently filters out the incoherent signal over the different modes (Tauzin et al., 2016).

Bin size is 2 km in horizontal direction and 1 km in vertical direction, similar to the study of Tauzin et al. (2016). The image is smoothed over 8 km horizontal and 3 km vertical distances (against 18 km and 8 km in Tauzin et al., 2016). We also muted the parts of the image where the combined coverage from Ps, PpPs, and PpSs phases is less than 10 rays. This processing allowed building and interpreting high-resolution images of the subducted JdF oceanic plate below the Cascadia forearc (Fig. 2d).

We interpreted the two multi-mode CCP images for central Oregon and northern California with a simple forward modeling
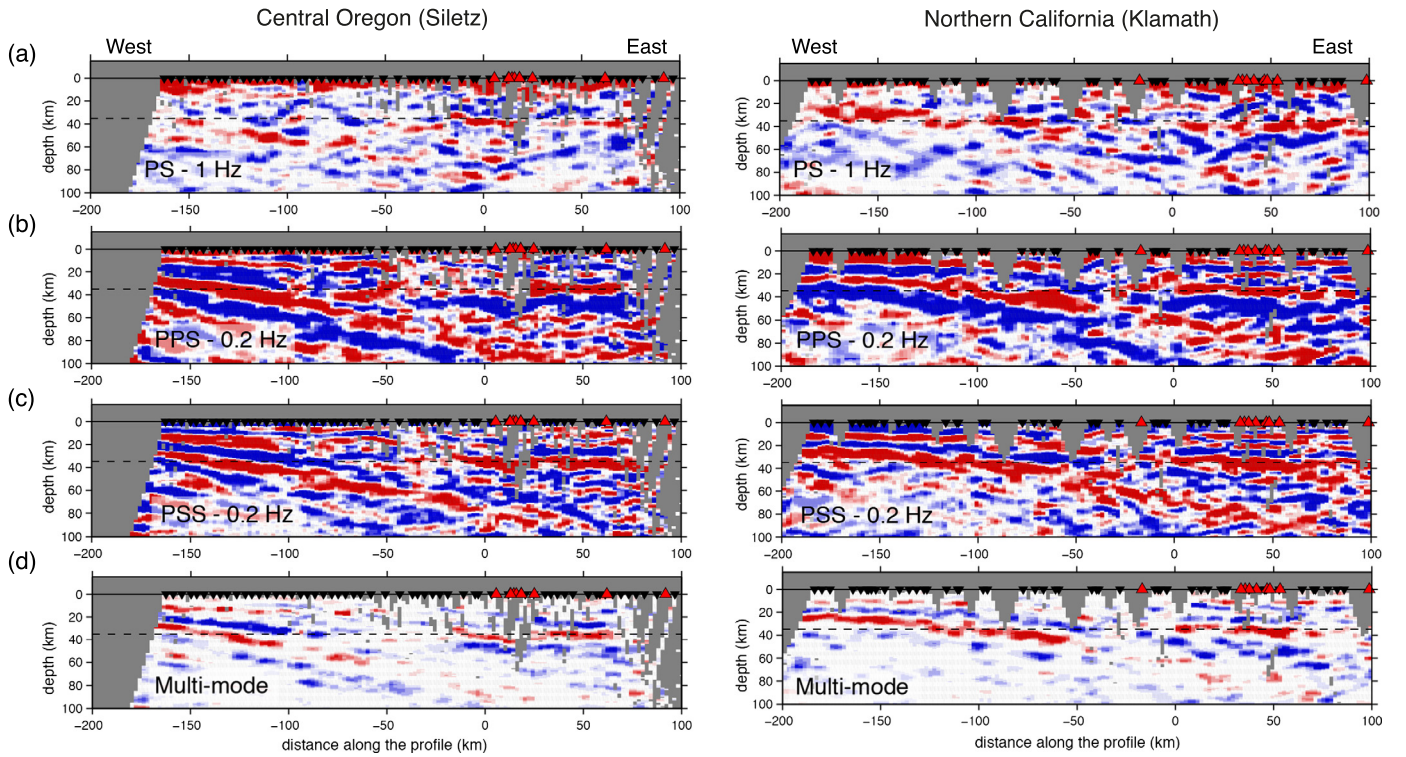
Fig. 2. Multi-mode conversion imaging of the Juan de Fuca plate in Central Oregon (left) and Gorda sub-plate in northern California (right). (a) Single mode high frequency (1 Hz) PS conversion images. (b) First multiple PPS images obtained at low-frequency (0.2 Hz). (c) Second multiple PSS images obtained at 0.2 Hz. The polarity has been reversed. (d) Multi-mode conversion images after phase-weighted stack (Tauzin et al., 2016). Red/blue colors indicate positive/negative seismic amplitudes with saturation at ±2.3% the P-wave amplitude. (For interpretation of the references to color in this figure legend, the reader is referred to the web version of this article.)
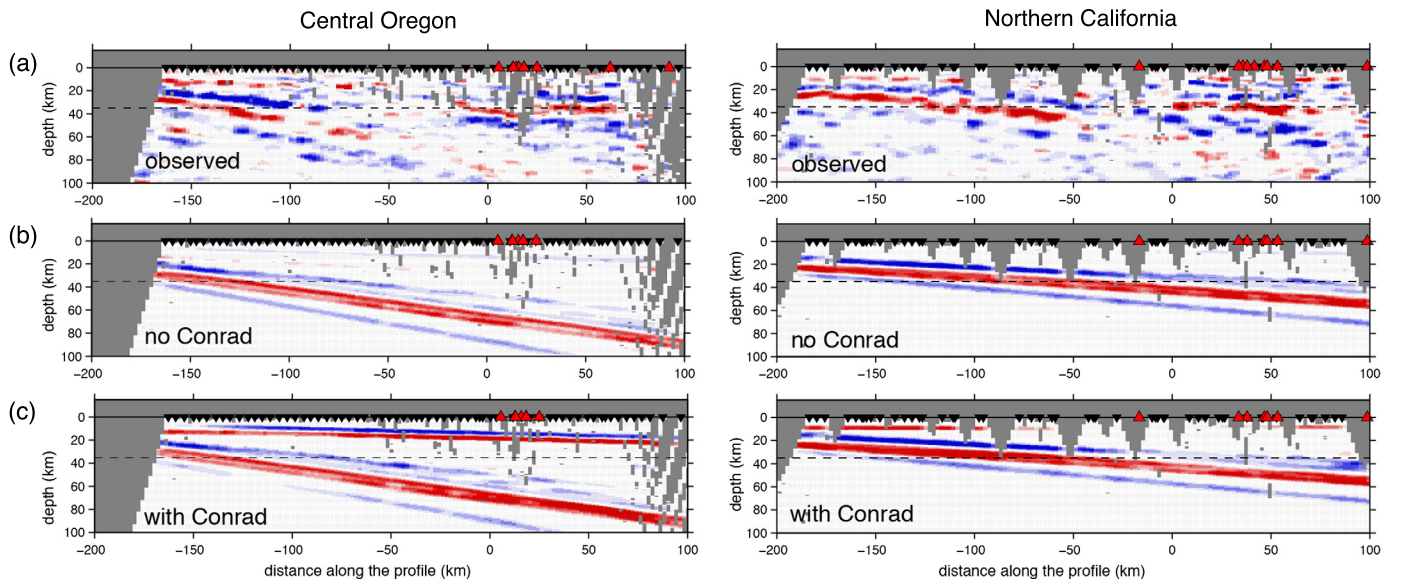
Fig. 3. Comparison of our seismic observations with the results of the synthetic modeling. (a) Our seismic observations for central Oregon (left) and northern California (right) (same as Fig. 2d). (b) Results of our modeling using the second input model where no interface (Conrad) is set in the crust. No fictitious interface appears near 15 km depth, suggesting that the mid-crustal discontinuity does not result from cross-mode contamination. (c) Result of our modeling using the first input model where an interface (the Conrad discontinuity) is set in the crust. We successfully recover the signature of the Conrad discontinuity. Red/blue colors indicate positive/negative seismic amplitudes with saturation at ±2.3% the P-wave amplitude. (For interpretation of the references to color in this figure legend, the reader is referred to the web version of this article.)

approach. That is, for each profile, we generated two synthetic CCP images from two subduction models including a dipping low-velocity layer in the mantle (the oceanic crust). In the first model, we set a positive interface in the crust of the overriding plate. In the second model, this intra-crustal interface is absent. The resulting images are shown and compared to the observations in Fig. 3. To construct these four synthetic images, seismograms were

generated for the same acquisition geometries as in central Oregon and northern California from a ray-based algorithm accounting for flat dipping stratifications (Frederiksen and Bostock, 2000). We used the IASP91 velocity model (Kennett and Engdahl, 1991) for time-to-depth conversion. For synthetic seismogram modeling, we manually adjusted the dip angle of the low-v_s oceanic layer and the values of v_s in the crust and mantle of models 1 and 2 so that
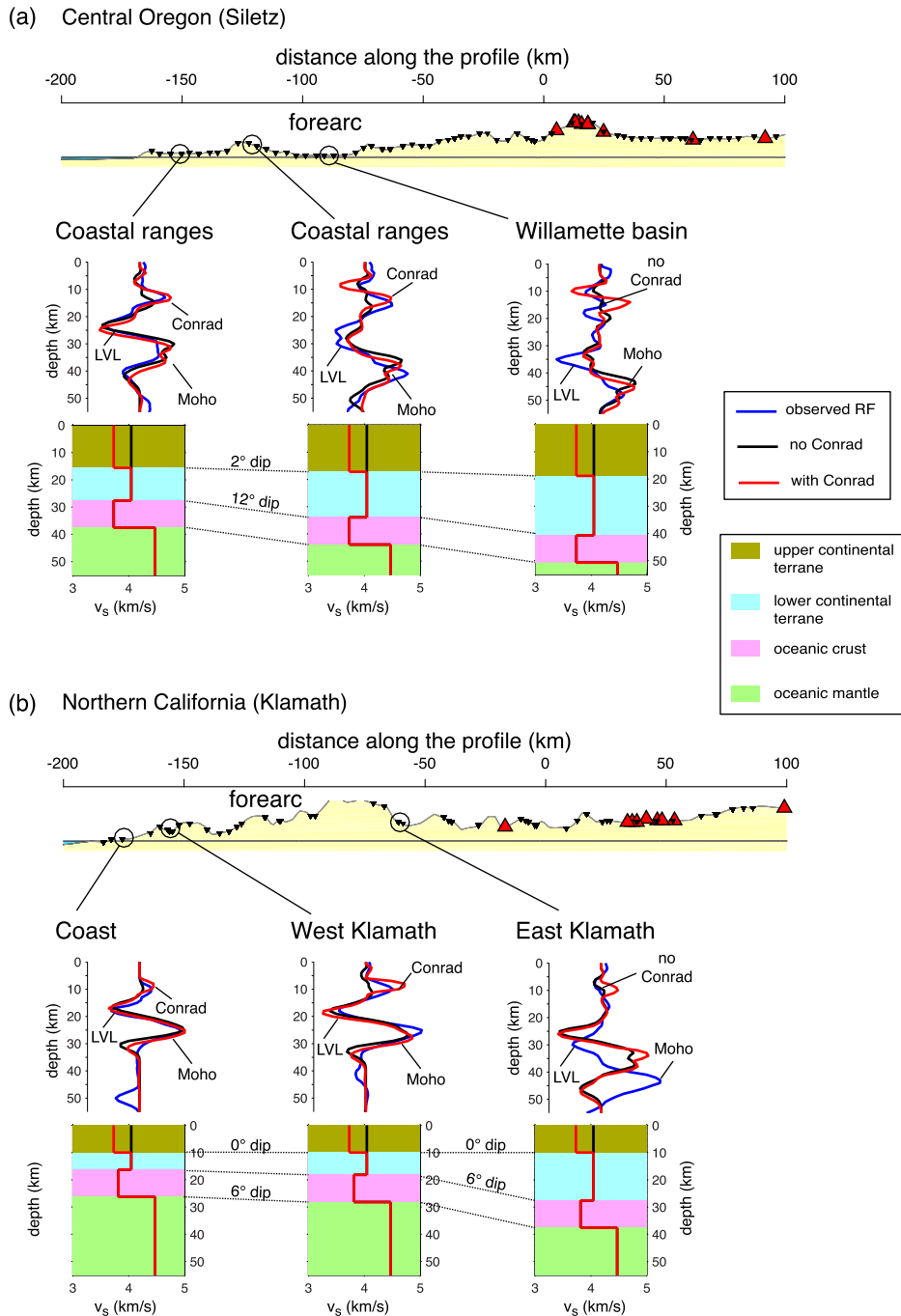
Fig. 4. Waveform modeling of the observed RFs. Blue waveforms are the observed stacked receiver functions; black and red waveforms are the receiver functions for the models shown with the same color on the bottom panel. The black model contains no mid-crustal (Conrad) discontinuity and the red contains a Conrad discontinuity. (a) Modeling results for the profile across central Oregon, with at left and middle the Coastal ranges and at right the Willamette Basin. (b) Same analysis performed on the data from the Klamath province (northern California). The waveforms marked as LVL correspond to the top of the oceanic crustal low-velocity layer. The fit of the LVL and the Moho is poor below the East Klamath Mountains in (b) because our two-dimensional modeling does not take into account the along-dip curvature of the seismic interfaces. (For interpretation of the references to color in this figure legend, the reader is referred to the web version of this article.)

the predicted RF amplitudes fit the amplitudes on the observed RFs (Fig. 4). Our best-fitting models for central Oregon and northern California are given in Tables 1 and 2. Amplitudes on the RFs are mainly sensitive to sharp v_s gradients so little constraints are obtained about the absolute velocities, v_p, or the density.

3. Results

The RF images (Figs. 5 and 6) reveal two eastward dipping discontinuities located near 30 km depth on the western side of both

profiles, one with a negative polarity interpreted as the top of the oceanic crust (Rondenay et al., 2001; Bostock et al., 2002), underlain by a positive discontinuity corresponding to the oceanic Moho. The two-dimensional forward waveform modeling (Fig. 4 and Tables 1–2) indicates that the shear velocity is reduced by ∼10% in the crustal oceanic layer, in agreement with former studies (Rondenay et al., 2001; Bostock et al., 2002). The low-v_s signature of the oceanic crust is attributed to the presence of hydrated minerals (Bostock et al., 2002; Hacker et al., 2003; Audet et al., 2009; Audet and Kim, 2016) and, where the fault zone is partially

Table 1
Parameters for the best fitting models in central Oregon. Receiver functions are sensitive to sharp changes of vs and little to the absolute values of velocities or the density.

Layer	Model-1				Model-2			
	Thickness (km)	v_p (km/s)	v_s (km/s)	Dip (°)	Thickness (km)	v_p (km/s)	v_s (km/s)	Dip (°)
Upper Terrane	14	6.7	3.7	0	–	–	–	–
Lower Terrane	11	7.2	4.0	2	25	7.2	4.0	0
Oceanic crust	10	6.7	3.7	12	10	6.7	3.7	12
Oceanic mantle	–	8.0	4.5	–	–	8.0	4.5	–

Table 2
Parameters for the best fitting models in northern California.

Layer	Model-1				Model-2			
	Thickness (km)	v_p (km/s)	v_s (km/s)	Dip (°)	Thickness (km)	v_p (km/s)	v_s (km/s)	Dip (°)
Upper Terrane	10	6.7	3.7	0	–	–	–	–
Lower Terrane	5	7.2	4.0	0	15	7.2	4.0	0
Oceanic crust	10	7.0	3.8	6	10	7.0	3.8	6
Oceanic mantle	–	8.0	4.5	–	–	8.0	4.5	–
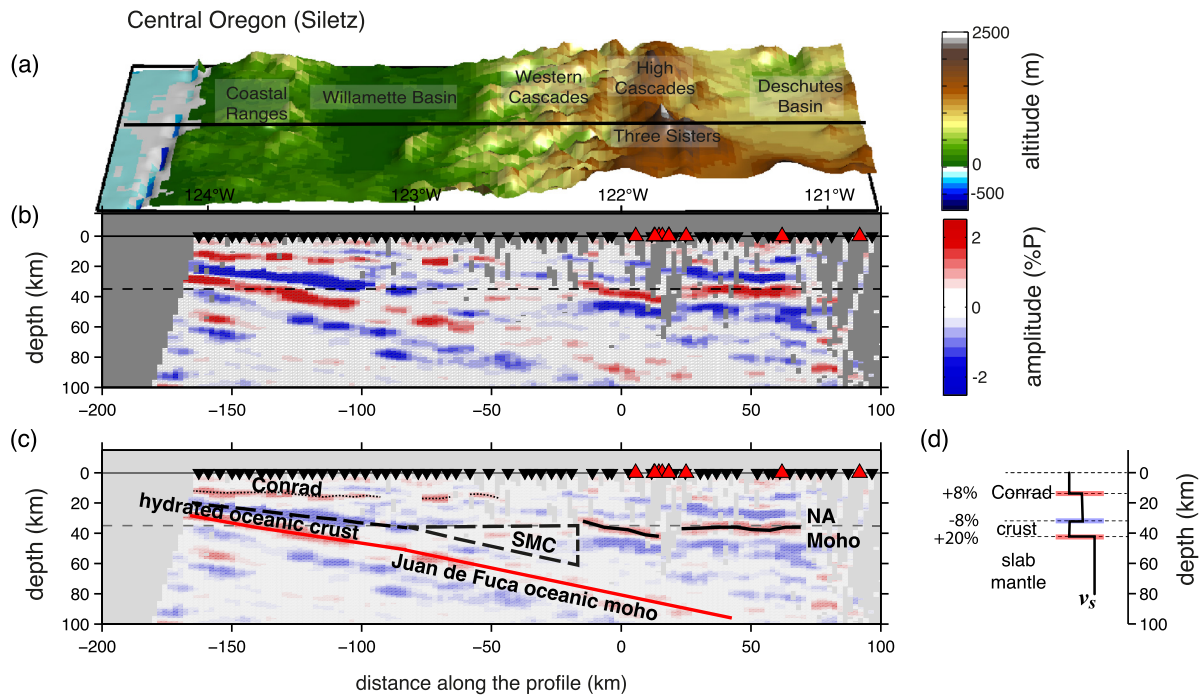
Fig. 5. (a) Topography of the area sampled by the seismic data in central Oregon (Siletz province). The black line marks the location of the seismic profile. (b) The raw seismic image of the Juan de Fuca plate obtained from multi-mode CCP stacking. Red/blue colors indicate downward increases/decreases of shear-wave velocity. Inverted black triangles and red triangles are seismic stations and volcanic centers projected onto the profile. The vertical exaggeration is 2/3. (c) Interpretation of the seismic image emphasizing the North American plate (NA) Moho at East, the serpentinized mantle corner (SMC) in the middle, and the hydrated Juan de Fuca oceanic crust at West. A positive interface appears at mid-crustal depth that we interpret as the Conrad discontinuity. The horizontal dashed lines mark the depth of 35 km. (d) A sketch of the radial shear-wave velocity model used for computing synthetic waveforms and fitting observed data in the forearc. This model is described in Table 1. (For interpretation of the references to color in this figure legend, the reader is referred to the web version of this article.)

sealed, with high-pore fluid pressure (Sleep and Blanpied, 1992; Audet et al., 2009). The low-v_s signature disappears near 40 km depth, below the Willamette Basin in Oregon (Fig. 5a, b), and beneath the northern limit of the Sacramento Valley in California (Fig. 6a, b). This observation has been attributed to crustal dehydration (eclogitization) (Bostock et al., 2002), resulting in the hydration (serpentinization) of a small corner of the mantle (SMC) above the descending slab. Serpentinization erases the signature of a portion of the continental NA Moho at the center of both profiles (Figs. 5b–c and 6b–c). These images of low-velocity zones and of the disappearance of the continental Moho are consistent with the

findings of previous regional seismic studies using inverse scattering (see Bostock, 2013, and references therein). We therefore focus on forearc features that have never been reported before.

A well-resolved seismic interface is observed at about 15 km depth in the crust of the overriding NA plate (Figs. 5b and 6b), as demonstrated by detailed analysis of observed RFs (Fig. 7) and by the synthetic tests (Figs. 3 and 4). For semantic convenience, we refer to this 15 km-discontinuity as the Conrad discontinuity whose nature is largely debated (Litak and Brown, 1989). This mid-crustal interface has been detected in other seismic studies (Park et al., 2004; Keach et al., 1989; Zucca et al., 1986;
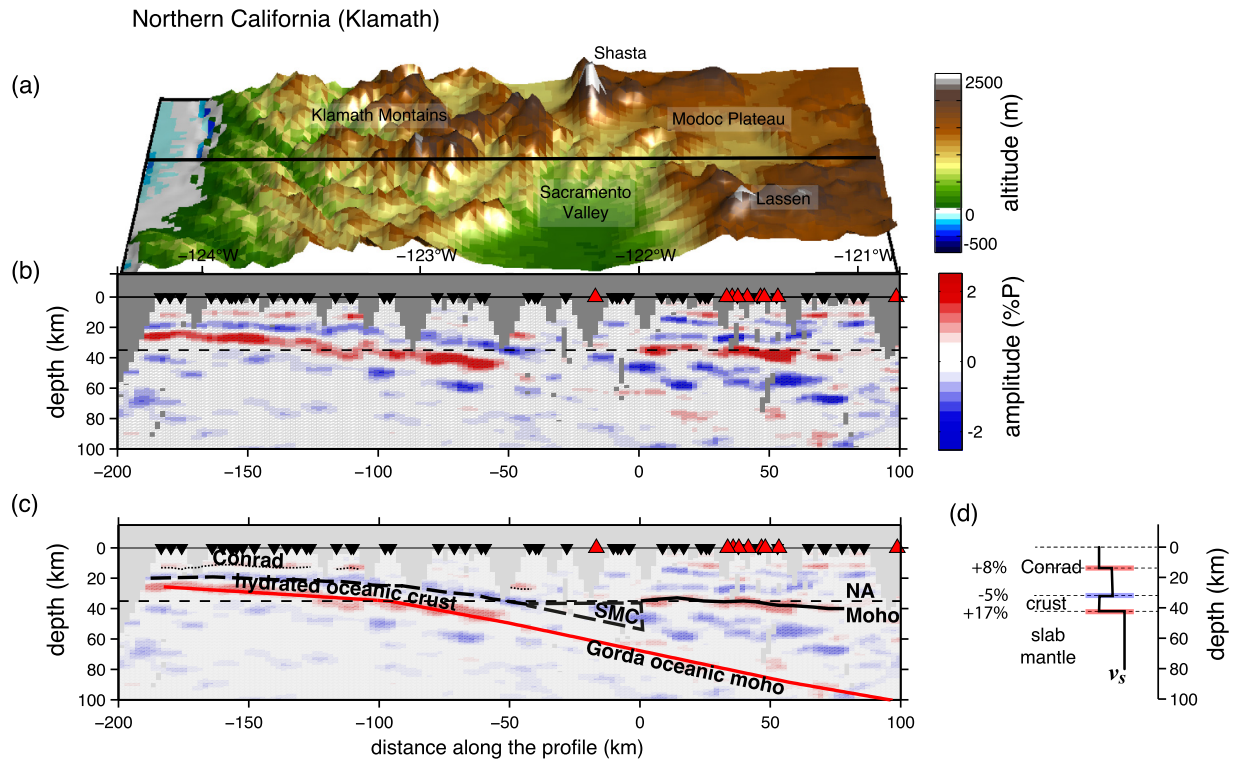
Fig. 6. Same as Fig. 5 except that the profile is obtained from the data in northern California (the Klamath province). The velocity model shown in (d) is described in Table 2.
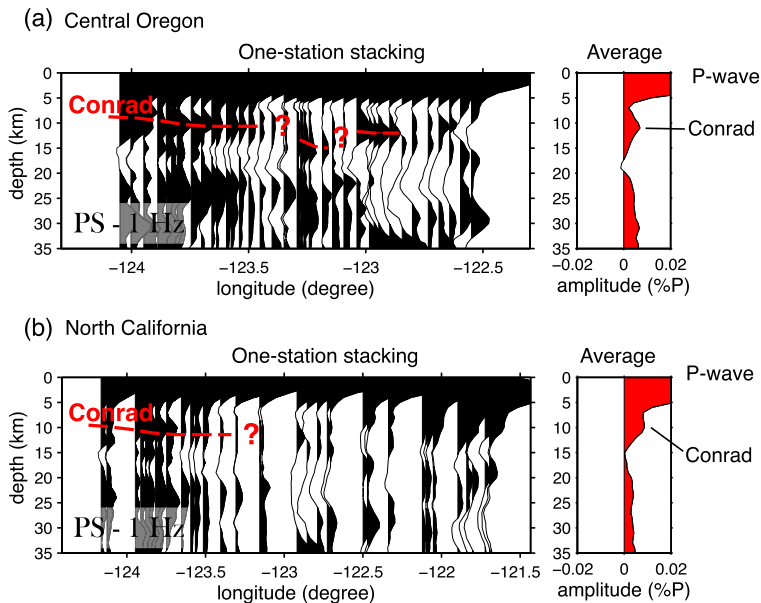

Fig. 7. Stack of receiver functions as a function of station longitude. (a) Profile across central Oregon. (b) Profile in northern California. The high-frequency (1 Hz) receiver functions are stacked after time-to-depth conversion in the IASP91 velocity model (Kennett and Engdahl, 1991). The sum of all the receiver functions for the two profiles is shown in the panels at right.

Trehu et al., 1994), and with the present observation, this demonstrates its large extent across the Cascadia forearc. Along both profiles, this interface is continuous to the West but exhibits significant gaps to the East (Figs. 5 and 6). In Oregon, the Conrad is segmented below and slightly east of the Willamette Basin. In California, the interface is continuous up to the summits of the Klamath Mountains where it is interrupted and re-appears east of the mountains (Figs. 5 and 6). Our two-dimensional forward modeling (Figs. 3 and 4) shows that, where observed, the Conrad discontinuity is associated with a ~8% increase of v_s with depth

in the crust of the overriding plates (Tables 1–2). Fig. 4 shows that the models do not require a v_s discontinuity below the Willamette basin and east of the Klamath Mountains, where the Conrad discontinuity is missing.

We note that several other discontinuities seem also present further East between 121–122°W below the arcs of Oregon and California. This includes a strong negative signal above the continental Moho in the High Cascades in Oregon (Fig. 5), two negative signals around 15 and 25 km depths and a positive signal at depth of ~10 km below the Modoc Plateau in California (Fig. 6).

4. On the robustness of the Conrad seismic signal

The Conrad discontinuity is not an artifact from our multi-mode CCP stacking approach. Our final images are constructed by stacking the three images obtained from the different modes. However, each individual image contains artifacts from other modes, *i.e.* parallel echoes of the real structure (Rondenay et al., 2001; Bostock et al., 2002; Nicholson et al., 2005; Abers et al., 2009). For example, PS conversions at the top and bottom of the low-v_s oceanic crust are mapped at shallower crustal depths in the image constructed with the PPS and PSS modes. This cross-mode contamination, if not corrected, could set a fictitious interface near 15 km depth, *i.e.* mimicking a Conrad discontinuity. Here, we have two arguments demonstrating that the observed Conrad discontinuity is a true feature, and not an artifact due to cross-mode contamination. First, the crude RF stacking and PS single-mode CCP stacking show a signal at mid-crustal depths (Figs. 2a and 7). As these images do not involve multiple-mode migration, these signals arise from direct conversions at a mid-crustal interface. Second, our synthetic tests (Figs. 3 and 4) show that in the case of the second input model where no interface is set in the crust, no fictitious interface appears near 15 km depth, suggesting that the PS energy converted from the Moho discontinuity is not mapped as a multiple at crustal depths.

Our simple forward modeling approach has however limitations because the ray-tracing algorithm allows us to account for flat dipping structure but not for variations in the dip of interfaces or reflectivity contrasts (Frederiksen and Bostock, 2000). Indeed, the top plate interface (negative amplitude) presents similar amplitudes as observed in the data in the western part of the profile beneath central Oregon (Fig. 3a-c), while it appears with weaker amplitudes further East (Fig. 3a-c). In northern California, our modeling does not also account for the changes in depth of the low-velocity layer and Moho below the East Klamath Mountains.

Our images display also some artifacts from the multi-mode stacking procedure (Tauzin et al., 2016). In both observed data in Fig. 3a (Oregon and California), the Conrad corresponds to a single discontinuity across which velocity increases with increasing depth. In our synthetic modeling for Central Oregon (Fig. 3c, left), a negative signal appears above the Conrad discontinuity. This negative signal is absent of the synthetic test for California (Fig. 3c, right). The major difference between these two synthetic tests is that we set a 12° dip for the Conrad discontinuity in Oregon compared to 6° in California (Tables 1–2). This imperfect recovery of the Conrad structure in Oregon results from the interference patterns between PS, PPS and PSS signals for dipping structures (see Tauzin et al., 2016, for details). The absence of this feature in observed data depends on the relative weight of the PS, PPS, and PSS signals in the multi-mode stacking.

5. Interpretation

The Conrad discontinuity has been attributed to different sources in the literature (see Litak and Brown, 1989, for a review): a boundary between a granitic upper crust and a basaltic lower crust, a metamorphic boundary between an upper crustal layer of amphibolite and a lower crustal layer of granulite, the transition from brittle behavior to ductile stretching, or a rheological barrier to upward migration of fluids. Whatever its origin, we use it here as a marker of the structural continuity of the terranes. The Conrad discontinuity seems indeed either internal to or delineating the base of accreted island arc-subduction terranes in the overriding NA plate (Zucca et al., 1986; Trehu et al., 1994; Blakely et al., 2005). Seismic refraction and gravity surveys (Zucca et al., 1986) indicate that the Klamath terrane in California is at

least 14 km thick (Zucca et al., 1986). In Oregon, seismic refraction lines (Trehu et al., 1994), RFs from the Corvallis permanent seismic station (Park et al., 2004), and gravimetric and aeromagnetic observations (Blakely et al., 2005), also require a structural boundary near 15 km depth that decomposes the ~34 km-thick Siletz terrane in two layers. As a marker of the terrane continuity, the Conrad segmentation would therefore indicate that these terranes are made of several tectonic blocks delimited by fracture zones.

At the current stage, providing a geological evidence supporting the existence of these deep fracture zones remains difficult: active seismic reflection campaigns (e.g. Keach et al., 1989) have limited depths of investigation and seismic refraction experiments (e.g. Zucca et al., 1986; Trehu et al., 1994) have poor lateral resolution, preventing from identifying the prolongation of surface geological structures down to a depth of 15 km (Fig. 8). However, in addition to our indirect observations, other geophysical data support the existence of deep fracture zones: the patterns in seismicity, non-volcanic tremors, and electrical conductivity in the forearc, as discussed in the next sections.

In the Californian arc, we doubt that the positive interface below the Modoc plateau is related to the Conrad discontinuity, for two reasons: (i) the history of volcanic and tectonic development of the Central High Cascade is complex (see e.g. Taylor, 1990) and may give rise to multiple seismic horizons (Fig. 6) unrelated to the structure of accreted terranes at West, and (ii) a seismic refraction experiment (Zucca et al., 1986) shows the existence of a crustal discontinuity below the arc in California, but the interpretation is that it is distinct from the ~15 km deep discontinuity in the forearc. To our knowledge there are no reports of the existence of negative discontinuities below the arc in central Oregon.

6. Implications for the hydrologic permeability and electrical conductivity of the forearc

We propose that the segmentation of accreted terranes controls fluid migration in the forearc (Fig. 9). This hypothesis is supported by correlations between seismic and magnetotelluric observations. We show in Fig. 10a images of the resistivity in the forearc obtained from the EMSLAB and KLMD magnetotelluric lines by Wannamaker et al. (2014). Both lines run from the coast to the volcanic arc (Figs. 1), but we make a qualitative comparison with our seismic observations only for the forearc portion (Fig. 10a, c). We superimpose our observed Conrad discontinuity (red line), to regular seismicity (black dots), and non-volcanic tremors (magenta stars). We also report the serpentinized mantle corner (SMC) inferred from our seismic observations.

The Conrad segmentation correlates with conductive regions of the forearc (Fig. 10a). High electrical conductivities are indicative of interconnected fluids in close association with the fracture zones. The terranes appear as large resistive blocks (~1000 Ωm) (Fig. 10a) with a thickness compatible with seismic and gravimetric data (Park et al., 2004; Keach et al., 1989; Zucca et al., 1986; Trehu et al., 1994; Blakely et al., 2005). Thus terrane blocks likely constitute large-scale permeability barriers to upward fluid migration (Wannamaker et al., 2014). In the Klamath province in California (Fig. 10a), the resistive blocks are narrower and the gap in the Conrad discontinuity is larger, suggesting that accreted terranes are more fractured and more permeable than the Siletz terrane in Oregon.

Fig. 9 summarizes the structural control of the terranes on fluid distribution in the Cascadia forearc. Potential fluid sources have two origins: the episodic release from the over-pressured dehydrating oceanic crust (Hacker et al., 2003; Audet et al., 2009), and focused flow from the downdip SMC within the sheared ser-
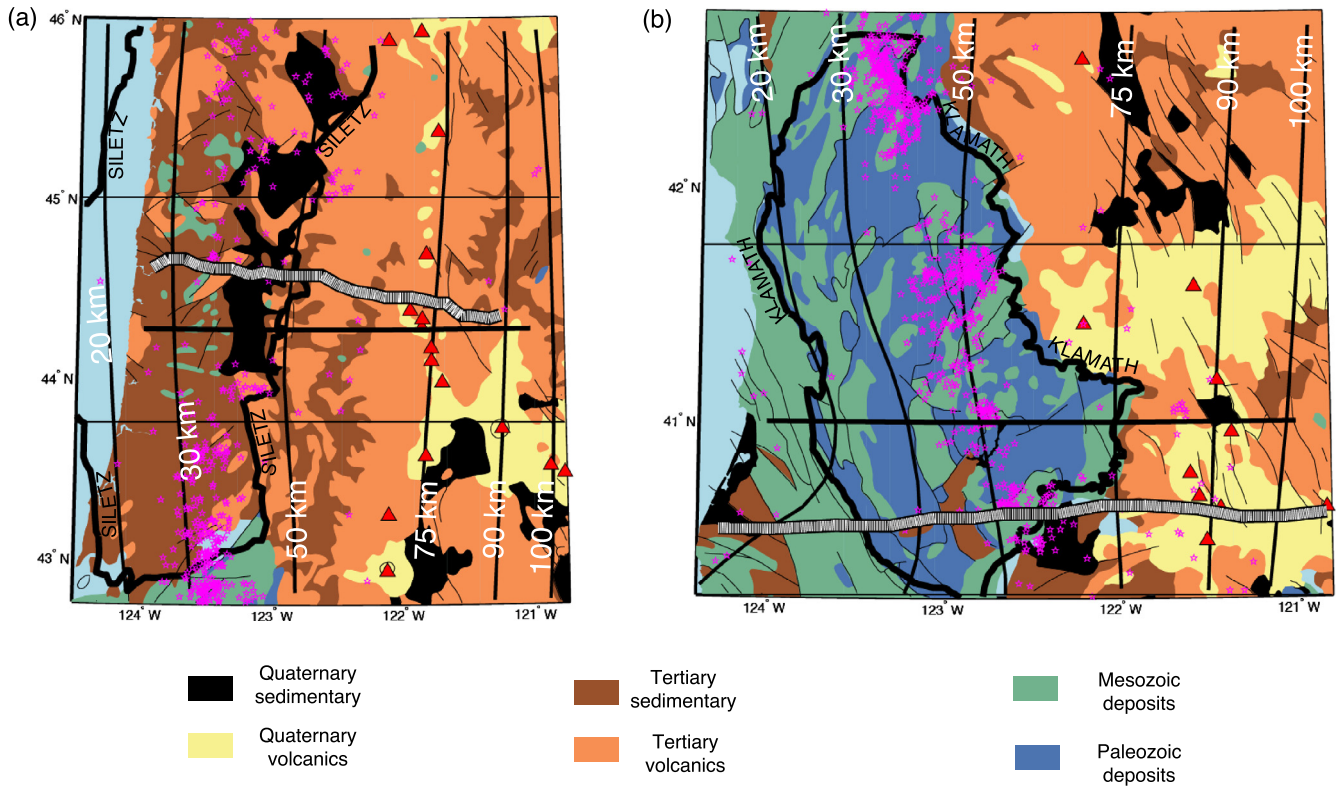
Fig. 8. (a–b) Zoom on the Oregon and California regions with the local geology (Schruben et al., 1994). The thick black lines at constant latitude correspond to the profiles used to create the seismic images. The thick black contours in the western part delimit the Siletz and Klamath geological terranes. The South–North black lines locate the depth of the top of the subducting Gorda–Juan de Fuca plate below the NA margin (McCrory et al., 2012). Large red triangles mark the location of Quaternary active volcanoes. The geographical location of non-volcanic tremors (Idehara et al., 2014) is shown with magenta stars. Surface faulting is indicated with the thin black lines on the geological units. Due to a lack of geophysical information, the prolongation of surface geological structures down to a depth of 15 km is uncertain. (For interpretation of the references to color in this figure legend, the reader is referred to the web version of this article.)

pentinized layer above the subduction interface (Kawano et al., 2011). Fluids are then collected at the base of the crust of the overriding plate, as evidenced by the medium and large amplitude conductive anomalies in Oregon and California, respectively, in Fig. 10a. In a recent model, Hyndman et al. (2015) proposed that the fluid from the dehydrating plate is focused and concentrated directly above the forearc SMC. Here, the combined interpretation of resistivity and seismic images rather suggests that the fluids are collected updip of the SMC (Fig. 10a). Fluids would then rise in the lower crust (Fig. 9), contributing to large-scale fluctuations of pore-fluid pressure (Sleep and Blanpied, 1992) possibly enhanced by SiO_2 precipitation (Audet and Bürgmann, 2014; Hyndman et al., 2015).

The fluids released from dehydration reactions of the oceanic crust have a low salinity and therefore cannot explain the observed high electrical conductivities (*e.g.* Reynard et al., 2011). This high-conductivity can result from the alteration of the crustal basement, as the reaction consumes the pure water component and leaves residual fluids enriched in salts (Scambelluri et al., 1997). Fluid volume fraction and salinity are not easy to constrain, both being the result of a complex history of water release, serpentinization and hydrothermal alteration of the deep crustal rocks. Observed conductivities in the lower crust of California would require saline brines with fluid fractions of ∼1% and NaCl molality of 0.3 to 1 m (Reynard, 2016). In Oregon, the higher resistivities are consistent with either lower fluid fractions (0.01–0.3%) at similar salinities, or lower salinities (<0.1 m) at similar fluid fractions (Reynard, 2016). In any case, higher fluid fractions in northern California are likely, and suggest that the forearc is more fractured and drained than in central Oregon (Fig. 9).

7. Discussion

7.1. Potential influence on the seismic cycle

The downdip seismogenic limit is where the fault zone no longer exhibits frictional instability. Among the factors that could affect this limit is the pore pressure on the fault (Hyndman, 2013). The structural difference between the Siletz and Klamath terranes could cause differential upward release of forearc fluids along the Cascadia margin, and may influence the seismic cycle by modulating both in time and space the slip behavior on the megathrust (Fig. 9).

Release of fluid pressure on the megathrust by percolation between blocks of terranes would result in locking the subduction interface by increasing the stress required for frictional failure. With smaller blocks and higher fracture density in accreted terranes, the plate interface would be better drained, hence more susceptible to earthquake failure in California than in Oregon. In the broad sealed areas of the Oregon megathrust where the Siletz terranes are thick and less permeable, the pore-fluid pressure is high and all the deformation could be continuously accommodated through stable sliding (Schmalzle et al., 2014). In this case, little slip would occur during large megathrust earthquakes, as modeled in Oregon for the magnitude ∼9.0 earthquake that ruptured the whole Cascadia margin in 1700 A.D. (Wang et al., 2013), suggesting that the locked portion was small in Oregon and located far offshore (Schmalzle et al., 2014). Conversely, the more permeable terranes of northern California would favor locking on a larger portion of the plate interface (Fig. 9) where large magnitude earthquakes have a ∼230-yr recurrence (Leonard et al., 2010). Finally, along-strike variations in pore-fluid pressures would pro-
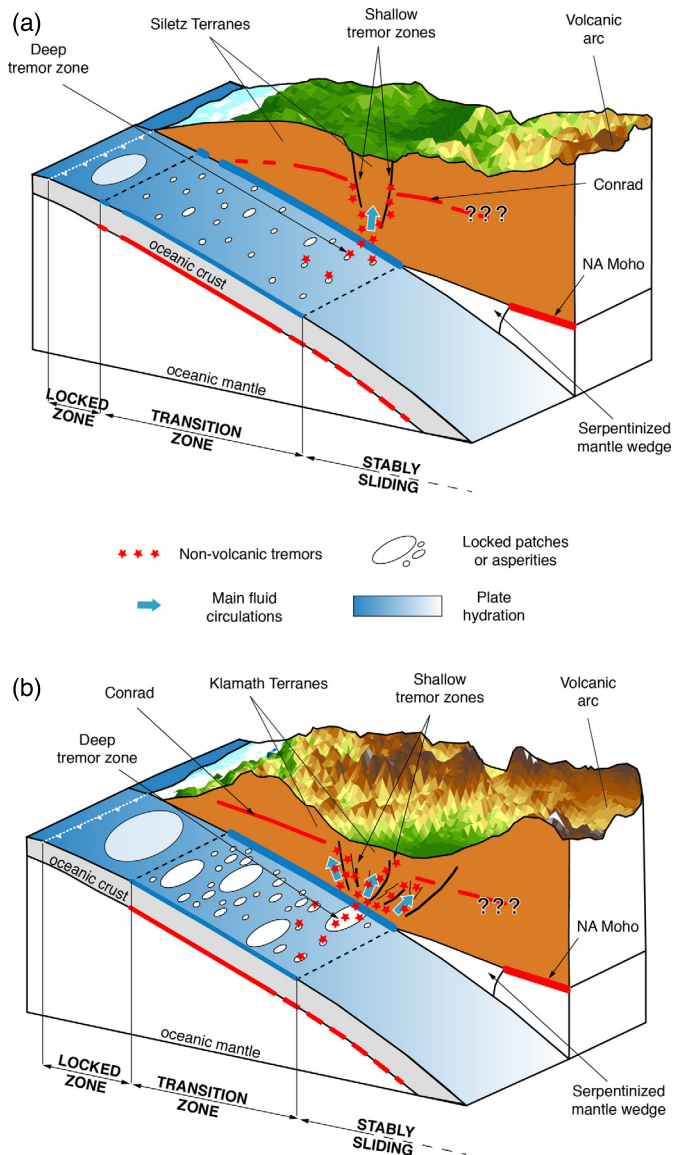
Fig. 9. A conceptual model summarizing the structural control of the terranes on fluid and seismicity distribution in the Cascadia forearc and on the frictional properties on the megathrust. (a) Because the terranes in Oregon are impermeable, pore-fluid pressure is high and the strength of the interface low, resulting in few small locked patches in the transition zone of the megathrust and a regime more favorable for stable sliding (Schmalzle et al., 2014). (b) In California, the forearc is heavily fractured and drained, resulting in lower pore-fluid pressure, and the development of larger high-friction patches on the transition zone of the megathrust. The downdip seismogenic limit (the boundary between the locked and transition zones) is shifted depending on the pore-pressure on the fault.

vide favorable conditions for generating aseismic slip and associated non-volcanic tremors (Obara, 2002; Rogers and Dragert, 2003; Kao et al., 2005; Ariyoshi et al., 2012) with variable recurrence intervals, as evidenced throughout the Cascadia forearc (Brudzinski and Allen, 2007).

7.2. The localization of non-volcanic tremors (NVTs)

The catalog that we used here (Idehara et al., 2014) shows a large NVT depth distribution (Fig. 10a) from the plate interface up to ∼15 km in the crust of the overriding plate. The shallow seismic activity aligns sub-vertically within the fracture zones evidenced by the gaps in the Conrad discontinuity (Fig. 10b and c). In Oregon, the NVTs are located in the gap below the Willamette Valley and, in California, a large swarm of NVTs extends through the gap of the

Conrad discontinuity between 123.15°W and 122.7°W (Fig. 10b, c). The NVTs spatially coincide with conductive anomalies in the fracture zones (Fig. 10a), whereas regular seismicity (McCrory et al., 2012) is mainly associated with a resistive signature, as observed in the western Cascades in Oregon (Fig. 10a). This suggests that some fractures take part of the large-scale hydrological network whereas others not.

There is a controversy on the location of tremors and related low-frequency earthquakes (Kao et al., 2005; La Rocca et al., 2009) because different localization methods have been used and have given different results. The principle consists in extracting travel-time differences between coherent patterns of waveforms across multiple stations and components. But a difference comes from the source function that is searched through the long and non-impulsive tremor signal. A first method, on which relies the catalog that we used here (Idehara et al., 2014), is based on the correlation of the envelope of horizontal components (Kao et al., 2005; Idehara et al., 2014; Ide, 2012). In Cascadia, it gives a large depth distribution of NVTs in the crust of the overriding plate (Figs. 10c). Another method identifies impulsive signals in the tremor signal by stacking and correlation across a network of stations (Shelly et al., 2007). The localization of NVTs using such a second type of method in northern California has been investigated by Plourde et al. (2015). Because the events appear located closer to a major structural boundary (the plate interface), this second method is believed to be more reliable and the current consensus is that NVTs locate primarily on the interplate boundary (Rogers and Dragert, 2003; La Rocca et al., 2009; Shelly et al., 2006).

However, if errors in the first method would affect the localization, they would apply over the whole NVT zone. This is not what is observed in California where the deep tremor zone is elongated over a large lateral distance, ∼50 km, but the shallow tremor zone has a narrower extension of ∼20 km, near 122.75°W longitude (Fig. 10a). In Oregon, the shallow tremor zone is also narrowly located toward the downstream of the plate interface, centered at ∼123.1°W longitude (Fig. 10a). Our study reveals in addition in California the striking spatial correlation of NVTs with conductive anomalies of the lower crust, at places marked by an absence of regular earthquakes (Fig. 10a). These observations support the idea that shallow crustal NVTs exist, and are related to well-connected fluid phases distributed across the fracture zones of the lower crust of the overriding plate (Kao et al., 2005).

8. Conclusion

The tectonic structure inherited from the geological history of the margin likely exerts on the seismic cycle a control as important as the amount of fluids that enters into the forearc through plate dehydration, or the roughness of the seafloor of the underthrusted plate. A correlation between the lithology of accreted terranes in the forearc and the frictional behavior of the megathrust was also recently evidenced in northeast Japan (Bassett et al., 2016). The fluid escape routes in the overriding plate bring saline brines near the surface where they can mix with meteoric waters in deep aquifers or in hydrothermal systems. Such a mixing was documented in the Willamette Basin in central Oregon (Hurwitz et al., 2005), and in the Arima hot springs in Japan above the Philippine plate (Kusuda et al., 2014), a subduction with a similar thermal regime as Cascadia. Systematic geophysical and geochemical investigation of hot springs, deep aquifers, and fracture zones in the overriding plate, should help unravel the important fluid cycle in the forearc region of subduction zones, and its potential influence on the seismic cycle.
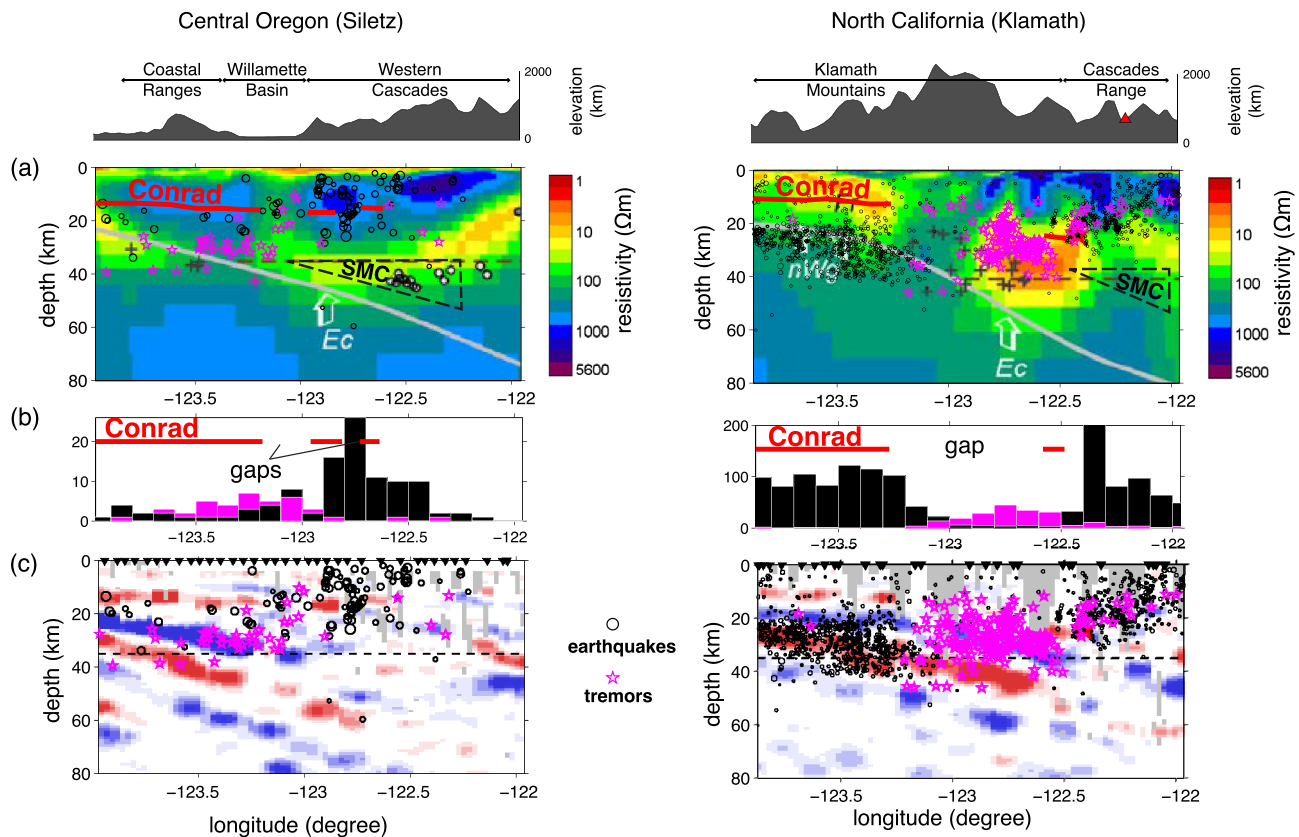
Fig. 10. (a) Resistivity profiles obtained from the EMSLAB and KLMD magnetotelluric lines (modified from Wannamaker et al., 2014) in Oregon (left) and California (right). Warm colors correspond to low resistivities (high conductivities). Earthquakes (black dots) and non-volcanic tremors (magenta stars) are superimposed. In California, only the closest tremor events to the KLMD line are plotted (Fig. 1). Deep long period and low frequency earthquakes are located with dark gray plus and circles. The outlined dashed triangles are the serpentinized mantle corners (SMC). The topographic profiles are shown at the top. The seismic line being far apart the KLMD magnetotelluric line in northern California, the Conrad discontinuity might not be associated with the observed high electrical conductivities in the Franciscan complex below the Klamath Mountains. The location of eclogitization (Ec) is marked by up-arrows according to the results of prior studies (Wannamaker et al., 2014), and are consistent with our seismic image in Oregon but not in California. (b) Histograms of the distribution of regular earthquakes (black) and non-volcanic tremors (magenta) along the profiles in Oregon (left) and California (right). (c) Zooms on the RF profiles of Figs. 5 (left) and 6 (right). Earthquakes (black dots) and non-volcanic tremors (magenta stars) are superimposed. The color-scale ranges between −2.3 and +2.3% the P-wave amplitude, as in Figs. 5 and 6. The horizontal black dashed lines mark the depth of 35 km. Earthquakes are from McCrory et al. (2012) and non-volcanic tremors are from Idehara et al. (2014). (For interpretation of the references to color in this figure legend, the reader is referred to the web version of this article.)

Acknowledgements

References

Abers, G.A., MacKenzie, L.S., Rondenay, S., Zhang, Z., Wech, A.G., Creager, K.C., 2009. Imaging the source region of Cascadia tremor and intermediate-depth earth-quakes. Geology 37 (12), 1119–1122.

Ammon, C., 1991. The isolation of receiver effects from teleseismic P waveforms. Bull. Seismol. Soc. Am. 81, 2504–2510.

Ariyoshi, K., Matsuzawa, T., Ampuero, J.-P., Nakata, R., Hori, T., Kaneda, Y., Hino, R., Hasegawa, A., 2012. Migration process of very low-frequency events based on a chain-reaction model and its application to the detection of preseismic slip for megathrust earthquakes. Earth Planets Space 64 (8), 693–702.

Audet, P., Bürgmann, R., 2014. Possible control of subduction zone slow-earthquake periodicity by silica enrichment. Nature 510 (7505), 389–392.

Audet, P., Kim, Y., 2016. Teleseismic constraints on the geological environment of deep episodic slow earthquakes in subduction zone forearcs: a review. Tectono-physics 670, 1–15.

Audet, P., Bostock, M.G., Christensen, N.I., Peacock, S.M., 2009. Seismic evidence for overpressured subducted oceanic crust and megathrust fault sealing. Nature 457 (7225), 76–78.

Bassett, D., Sandwell, D.T., Fialko, Y., Watts, A.B., 2016. Upper-plate controls on co-seismic slip in the 2011 magnitude 9.0 Tohoku-Oki earthquake. Nature 531 (7592), 92–96.

Blakely, R.J., Brocher, T.M., Wells, R.E., 2005. Subduction-zone magnetic anomalies and implications for hydrated forearc mantle. Geology 33 (6), 445–448.

Bostock, M., 2013. The Moho in subduction zones. Tectonophysics 609, 547–557.

Bostock, M., Hyndman, R., Rondenay, S., Peacock, S., 2002. An inverted continental Moho and serpentinization of the forearc mantle. Nature 417 (6888), 536–538.

Brudzinski, M.R., Allen, R.M., 2007. Segmentation in episodic tremor and slip all along Cascadia. Geology 35 (10), 907–910.

Dragert, H., Wang, K., James, T.S., 2001. A silent slip event on the deeper Cascadia subduction interface. Science 292 (5521), 1525–1528.

Ernst, W., Snow, C.A., Scherer, H.H., 2008. Contrasting early and late mesozoic petrotectonic evolution of northern California. Geol. Soc. Am. Bull. 120 (1–2), 179–194.

Frederiksen, A., Bostock, M., 2000. Modelling teleseismic waves in dipping anisotropic structures. Geophys. J. Int. 141, 401–412.

Hacker, B.R., Peacock, S.M., Abers, G.A., Holloway, S.D., 2003. Subduction factory, 2: are intermediate-depth earthquakes in subducting slabs linked to metamorphic dehydration reactions? J. Geophys. Res., Solid Earth 108 (B1).

Hetényi, G., 2007. Evolution of Deformation of the Himalayan Prism: From Imaging to Modelling. Ph.D. thesis. Université Paris Sud-Paris XI.

Hurwitz, S., Mariner, R.H., Fehn, U., Snyder, G.T., 2005. Systematics of halogen ele-ments and their radioisotopes in thermal springs of the cascade range, central Oregon, western USA. Earth Planet. Sci. Lett. 235 (3), 700–714.

Hyndman, R.D., 2013. Downdip landward limit of Cascadia great earthquake rupture. J. Geophys. Res., Solid Earth 118 (10), 5530–5549.

Hyndman, R.D., McCrory, P., Wech, A., Kao, H., Ague, J., 2015. Cascadia subducting plate fluids channelled to fore-arc mantle corner: ETS and silica deposition. J. Geophys. Res., Solid Earth 120 (6), 4344–4358.

Ide, S., 2012. Variety and spatial heterogeneity of tectonic tremor worldwide. J. Geophys. Res., Solid Earth 117 (B3).

Idehara, K., Yabe, S., Ide, S., 2014. Regional and global variations in the temporal clustering of tectonic tremor activity. Earth Planets Space 66 (1), 1–10.

Kao, H., Shan, S.-J., Dragert, H., Rogers, G., Cassidy, J.F., Ramachandran, K., 2005. A wide depth distribution of seismic tremors along the northern Cascadia margin. Nature 436 (7052), 841–844.

Kawano, S., Katayama, I., Okazaki, K., 2011. Permeability anisotropy of serpentinite and fluid pathways in a subduction zone. Geology 39 (10), 939–942.

Keach, R.W., Oliver, J., Brown, L., Kaufman, S., 1989. Cenozoic active margin and shallow cascades structure: COCORP results from western Oregon. Geol. Soc. Am. Bull. 101 (6), 783–794.

Kennett, B., Engdahl, E., 1991. Travel times for global earthquake location and phase identification. Geophys. J. Int. 105, 429–465.

Kusuda, C., Iwamori, H., Nakamura, H., Kazahaya, K., Morikawa, N., 2014. Arima hot spring waters as a deep-seated brine from subducting slab. Earth Planets Space 66 (1), 1–13.

La Rocca, M., Creager, K.C., Galluzzo, D., Malone, S., Vidale, J.E., Sweet, J.R., Wech, A.G., 2009. Cascadia tremor located near plate interface constrained by *S* minus *P* wave times. Science 323 (5914), 620–623.

Leonard, L.J., Currie, C.A., Mazzotti, S., Hyndman, R.D., 2010. Rupture area and displacement of past Cascadia great earthquakes from coastal coseismic subsidence. Geol. Soc. Am. Bull. 122 (11–12), 2079–2096.

Ligorrìa, J., Ammon, C., 1999. Iterative deconvolution and receiver-function estimation. Bull. Seismol. Soc. Am. 85, 1395–1400.

Litak, R.K., Brown, L.D., 1989. A modern perspective on the Conrad discontinuity. Eos 70 (29), 713–725.

McCrory, P.A., Blair, J.L., Waldhauser, F., Oppenheimer, D.H., 2012. Juan de Fuca slab geometry and its relation to Wadati–Benioff zone seismicity. J. Geophys. Res., Solid Earth 117. B9.

McCrory, P.A., Wilson, D.S., 2013. A kinematic model for the formation of the Siletz-Crescent forearc terrane by capture of coherent fragments of the Farallon and Resurrection plates. Tectonics 32 (3), 718–736.

Nicholson, T., Bostock, M., Cassidy, J., 2005. New constraints on subduction zone structure in northern Cascadia. Geophys. J. Int. 161 (3), 849–859.

Obara, K., 2002. Nonvolcanic deep tremor associated with subduction in southwest Japan. Science 296 (5573), 1679–1681.

Park, J., Yuan, H., Levin, V., 2004. Subduction zone anisotropy beneath Corvallis, Oregon: a serpentinite skid mark of trench-parallel terrane migration? J. Geophys. Res., Solid Earth 109 (B10).

Plourde, A.P., Bostock, M.G., Audet, P., Thomas, A.M., 2015. Low-frequency earthquakes at the southern Cascadia margin. Geophys. Res. Lett. 42 (12), 4849–4855.

Reynard, B., 2016. Mantle hydration and Cl-rich fluids in the subduction forearc. Prog. Earth Planet. Sci. 3 (1), 1.

Reynard, B., Mibe, K., Van de Moortèle, B., 2011. Electrical conductivity of the serpentinised mantle and fluid flow in subduction zones. Earth Planet. Sci. Lett. 307 (3), 387–394.

Reyners, M., Eberhart-Phillips, D., 2009. Small earthquakes provide insight into plate coupling and fluid distribution in the Hikurangi subduction zone, New Zealand. Earth Planet. Sci. Lett. 282 (1), 299–305.

Rogers, G., Dragert, H., 2003. Episodic tremor and slip on the Cascadia subduction zone: the chatter of silent slip. Science 300 (5627), 1942–1943.

Rondenay, S., Bostock, M., Shragge, J., 2001. Multiparameter two-dimensional inversion of scattered teleseismic body waves, 3: application to the Cascadia 1993 data set. J. Geophys. Res., Solid Earth 106 (B12), 30795–30807.

Scambelluri, M., Piccardo, G.B., Philippot, P., Robbiano, A., Negretti, L., 1997. High salinity fluid inclusions formed from recycled seawater in deeply subducted alpine serpentinite. Earth Planet. Sci. Lett. 148 (3), 485–499.

Schimmel, M., Paulssen, H., 1997. Noise reduction and detection of weak, coherent signals through phase-weighted stacks. Geophys. J. Int. 130 (2), 497–505.

Schmalzle, G.M., McCaffrey, R., Creager, K.C., 2014. Central Cascadia subduction zone creep. Geochem. Geophys. Geosyst. 15 (4), 1515–1532.

Schruben, P.G.A., Bawiec, R.E., King, W.J., Beikman, P.B., Helen, M., 1994. Geology of the conterminous united states at 1:2,500,000 scale – a digital representation of the 1974 P.B. King and H.M. Beikman map.

Shelly, D.R., Beroza, G.C., Ide, S., 2007. Non-volcanic tremor and low-frequency earthquake swarms. Nature 446 (7133), 305–307.

Shelly, D.R., Beroza, G.C., Ide, S., Nakamula, S., 2006. Low-frequency earthquakes in Shikoku, Japan, and their relationship to episodic tremor and slip. Nature 442 (7099), 188–191.

Sleep, N.H., Blanpied, M.L., 1992. Creep, compaction and the weak rheology of major faults. Nature 359 (6397), 687–692.

Tauzin, B., Bodin, T., Debayle, E., Perrillat, J.-P., Reynard, B., 2016. Multi-mode conversion imaging of the subducted Gorda and Juan de Fuca plates below the north American continent. Earth Planet. Sci. Lett. 440, 135–146.

Tauzin, B., Van Der Hilst, R.D., Wittlinger, G., Ricard, Y., 2013. Multiple transition zone seismic discontinuities and low velocity layers below western United States. J. Geophys. Res., Solid Earth 118 (5), 2307–2322.

Taylor, E.M., 1990. Volcanic history and tectonic development of the central high cascade range, Oregon. J. Geophys. Res., Solid Earth 95 (B12), 19611–19622.

Trehu, A., Asudeh, I., Brocher, T., Luetgert, J., Mooney, W., Nabelek, J., Nakamura, Y., et al., 1994. Crustal architecture of the Cascadia forearc. Science 266 (5183), 237–243.

Wang, P.-L., Engelhart, S.E., Wang, K., Hawkes, A.D., Horton, B.P., Nelson, A.R., Witter, R.C., 2013. Heterogeneous rupture in the great Cascadia earthquake of 1700 inferred from coastal subsidence estimates. J. Geophys. Res., Solid Earth 118 (5), 2460–2473.

Wannamaker, P.E., Evans, R.L., Bedrosian, P.A., Unsworth, M.J., Maris, V., McGary, R.S., 2014. Segmentation of plate coupling, fate of subduction fluids, and modes of arc magmatism in Cascadia, inferred from magnetotelluric resistivity. Geochem. Geophys. Geosyst. 15 (11), 4230–4253.

Wittlinger, G., Vergne, J., Tapponnier, P., Farra, V., Poupinet, G., Jiang, M., Su, H., Herquel, G., Paul, A., 2004. Teleseismic imaging of subducting lithosphere and Moho offsets beneath western Tibet. Earth Planet. Sci. Lett. 221, 117–130.

Zhu, L., 2000. Crustal structure across the San Andreas fault, southern California, from teleseismic converted waves. Earth Planet. Sci. Lett. 179, 183–190.

Zucca, J.J., Fuis, G.S., Milkereit, B., Mooney, W.D., Catchings, R.D., 1986. Crustal structure of northeastern California. J. Geophys. Res., Solid Earth 91 (B7), 7359–7382.